PNC TN 6410 92－004

公開資料

# ESR and cathodoluminescence studies of radiation defects in clays and quartz from some U deposits.

1992年3月

動力炉・核燃料開発事業団

人 形 峠 事 業 所

# 電子スピン共鳴分光法及びカソードルミネッセンス法による ウラン鉱床産粘土鉱物及び石英の放射線損傷の研究

ブランディーヌ　クローゼル・小室　光世・
中嶋　悟・永野　哲志・正木　信行・林　久人

## 要旨

主に堆積岩中に胚胎する世界のウラン鉱床6地域の岩石試料について，鉱物の放射線損傷を電子スピン共鳴分光法(ESR)及びカソードルミネッセンス(CL)法により調べた．カオリン鉱物を含む粘土フラクション粉体のESRスペクトルには，カオリナイトに知られている放射中心と同様のシグナルが観察された．しかし，他のスメクタイトやイライト等の粘土鉱物にはこのような放射中心は認められなかった．従って，岩石の風化や変質の際の，ウラン等の放射性元素の挙動の指標としては，カオリン鉱物が最も適している．同じ試料薄片のCL法による観察では，ウランの含有量の高い試料中の石英粒子の周縁部に，30ミクロン程度の放射線損傷リムが存在していることが観察された．このリムは，ウランの含有量が低くても年代の古い試料には存在しており，石英の堆積時から現在までの放射線被爆歴を示している．従って，これら2つの手法は，鉱床生成時から現在にかけてのウランの2次的移動・濃集過程の解析の手段として用いる事ができる．

Manuscript submitted to
*Rept. Res. Inst. Natural Resources, Mining Coll. Akita Univ.*, No.57,
##-##, March 1992
Final Version: March 5, 1992.

# ESR and cathodoluminescence studies of radiation defects in clays and quartz from some U deposits.

Blandine CLOZEL*, Kosei KOMURO***,
Satoru NAKASHIMA**** , Tetsushi NAGANO*, Nobuyuki MASAKI**
and Hisato HAYASHI****

(accepted ## #, 1992)

## Abstract

Rock samples from different world U deposits mainly in sedimentary rocks have been studied by Electron Spin Resonance (ESR) spectroscopy and Cathodoluminescence (CL) measurement in order to characterize radiation damage centers in clays and quartz. The presence of kaolinite-like radiation centers in ESR spectra in some of the samples containing kaolin group minerals suggests that this type of radiation damages can be used as an indicator of U behavior during supergene and hydrothermal alteration of U ores. Other clay minerals such as smectite and illite were not found to exhibit radiation damage centers by ESR. CL measurement on quartz grains indicated the presence of radiation damage rims for the samples containing high U content. These rims can also be recognized for older samples with low U concentration because of the longer contact of quartz with U. Although much more systematic studies are need for the reconstruction of the U behavior, these two methods have been proven useful for the characterization of radiation damage histories recorded in minerals.

---

* Environmental Geochemistry Laboratory and
** Radiochemistry Laboratory, Japan Atomic Energy Research Institute, Tokai, Ibaraki 319-11, Japan,
*** Waste Isolation and Ore Processing Division, Power Reactor and Nuclear Fuel Development Corporation, Okayama 708-06,Japan,
**** Research Institute of Natural Resources, Mining College, Akita University, Akita 010, Japan.

## 1.Introduction

The behavior of uranium through the earth's history includes a wide variety of processes such as the evolution of the atmosphere, the oceans, organic matter and the crust. The global geochemical cycle of uranium can be hence a significant benchmark of geohistory. Some of the world largest U deposits were found in sedimentary environments often associated with carbonaceous materials (Nakashima, 1991c). Uranium is first enriched in the sedimentary rocks by means of adsorption and reduction processes by organic matter, clays and zeolites in a reducing environment (Doi et al., 1975, Doi and Hirono, 1990; Maynard, 1983; Nakashima et al., 1984 and 1987, Nakashima, 1992a,b). The changes in physicochemical and hydrogeologic environments such as the penetration of hydrothermal solution or groundwater will induce a secondary migration of U. Some of primary U minerals (reduced type ore) are leached and precipitated as secondary uranyl minerals (oxidized type ore). U behavior from the primary deposition through the present time hence includes a series of U input and output. The knowledge of these processes are very important in the assessment of U ore deposits. Recently, this geochemical cycling of U has called much attention in the safety assessment of the geological disposal of high-level radioactive waste (Nakashima, 1990, 1991b and 1991c).

The complex U behavior in a geological time scale often hinders its reconstitution by means of conventional mineralogical and petrological analyses, since U minerals and their mode of occurrence and textures now observed are only the final state of a series of U migration/fixation processes. New methodologies are hence needed to understand better the paleo-behavior of U. U is one of the radioactive elements emitting $\alpha$, $\beta$ or $\gamma$-rays which irradiate the minerals nearby. Radiation damage centers recorded in minerals associated with U deposits will provide us with information on the history of radiation damages received from radionuclides. These radioactive elements can be coming into or escaping from the site with a close relation to the formation of secondary minerals.

Electron Spin Resonance (ESR) spectroscopy is based on the presence of unpaired electron in materials and has been used in mineralogy for the analyses of crystal chemistry of paramagnetic species having d (transition elements) or f electrons (rare earths and actinides) (Marfunin, 1979; Calas, 1988) and also color centers including radiation damages in minerals (Marfunin, 1979; Calas, 1988). However, the characterization of radiation damages by ESR has been limited mainly to quartz and zircon. Clay minerals are abundant in the world largest U deposits and closely related to the U migration. Among them, kaolinite has been found to give radiation defect signals by ESR (Hall, 1980 a,b; Muller and Calas, 1989; Clozel, 1991).

Recently, ESR spectroscopy on kaolinite from some U mineralized area in the world has been extensively studied by Clozel (1991). Kaolinite exhibits three types of radiation damage centers. The nature of these centers

have been hypothesized as follows based on irradiation and thermal annealing experiments. One of them named A center is the most stable one and can be reproduced by ionization through γ irradiation and implantation of $He^+$. This center is considered to conserve a memory of irradiation for the period superior to 1 million of years (1 Ma) at 80 °C. A' center is stable probably for the period between one hundred and several thousands of years at around 25 °C and several years at 80 °C. This center is selectively created by implantation of $He^+$ and $Pb^{2+}$ and so that related to the atom displacement associated with α-recoil. B center is the most unstable one and have its stability for the period of 10 to 100 years at around 25 °C and several months at 80 °C so that is an indicator of a recent irradiation. This center can be reproduced by the ionization through γ irradiation and implantation of $He^+$. Consequently, ESR studies on kaolinite from U deposits can provide us with useful constraints on the time scale of paleo-presence of U.

Following the detailed studies already undertaken on natural kaolinite samples from two Brazilian supergene U deposits (Muller et al., 1992) and one Mexican hydrothermal U deposit (Ildefonse et al., 1990; 1991) for the characterization of radiation centers, we can now expect to have radiation damage records in kaolin-like clays from a variety of more common U deposit samples.

Cathodoluminescence (CL) of minerals is observed for certain minerals when we irradiate them by electron beams under an optical or an electron microscope. This process uses a high excitation density via the conduction band and so that provides often much more intense luminescence signals than the excitation by ultraviolet (UV) light (photoluminescence, PL) or by heating (thermoluminescence, TL). The CL phenomenon of minerals is related to defect centers such as radiation damages and also to some trace amounts of transition elements such as Mn and Fe (Walker, 1985).

Most common mineral showing CL due to its defect centers is quartz. Two main CL has been observed for quartz in the visible wavelength region. One is a blue CL emission around 450 nm (2.7 eV) and the other is a red emission around 650 nm (1.9 eV) and these CL bands have been correlated with the corresponding ESR signals of quartz. The blue one is suggested to be due to a hole capture of E' center associated with an oxygen vacancy in Si-O-Si. The red one is suggested to be an oxygen-associated hole center (OHC) of a non-bridging oxygen which is preferably bonded to H to form OH bonds. This red emission has been known to be induced by irradiation by neutron and γ-rays(Walker, 1985).

CL measurement on some quartz grains have shown the presence of radiation damage rims on their outer surfaces (Smith and Stenstrom, 1965; Owen, 1988; Meunier et al.,1990). These damage rims are considered to be formed by irradiation with α-particles emitted by U and Th series radionuclides, because of similarities of their width, concentric ring structure and associated accessory minerals to pleochroic haloes in biotite (Owen,

1988). In the study of uranium ores, Komuro et al.(1992a in prep.) suggest that the analysis of damage rims by CL combined with a compositional mapping by EPMA provides unique data on ancient episodes of uranium removal.

These two different methods (ESR and CL) are hence considered to be useful in characterizing radiation damages for minerals associated with U deposits. The originality of the present paper is to combine for the first time these two methods for the study of radiation damages in minerals and to provide some constraints on U behavior through geologic time scale.

In this paper, 15 samples from 6 different uranium deposits mainly in sedimentary rocks of the world were studied by ESR for the radiation damage centers recorded in clays and by CL for the damages recorded in quartz. Clay fractions of interest are generally alteration products of either supergene or hydrothermal origin and are often related to U fixation or removal processes. On the other hand, quartz grains are unaltered parts of the rocks and their CL data will show the radiation environment history from their first contact with U after the sedimentation through the present time. Consequently, the combination of ESR and CL data together with the U content data of the bulk rocks will give us constraints on U behavior through the sedimentation, alteration, mineralization and remobilization. The compositional mapping by X-ray microanalyzer (EPMA) was also carried out on the same thin sections as those analyzed by CL. However, detailed discussion of combined CL and EPMA data will be published elsewhere (Komuro et al., 1992a in prep.).

## 2.Samples

Rock samples used in the present study were originated from 6 uranium mineralized areas in the world. Their geological settings and modes of U occurrence are briefly described in Table 1.

Sample Nos. 10, 2 and 15 are from Ningyo-toge mine, Okayama, Japan. This deposit is in Tertiary (Miocene to Pliocene) conglomerate-sandstone between overlaying shale - pyroclastics and a granitic basement. U is present as autunite, nyngyoite and uraninite and is considered to be mineralized through a repetitive adsorption-reduction of U in groundwater mainly by carbonaceous materials including its leaching episodes (Doi and Hirono, 1990).

Sample Nos. 3, 14, 11, 13 and 6 are from Tono Mine, Gifu, Japan. U is mineralized as autunite, coffinite, uraninite and uranocircite in Miocene conglomerate-sandstone between overlaying pyroclastics and a granitic basement. The genetic model for Tono as a groundwater-channel deposit is almost the same as that for Ningyo-toge deposit (Doi and Hirono, 1990). Recent microscopic studies on some of these samples indicate that U is found as coffinite or pitchblende in smectites filling interstices of the detrital grains and altered parts of biotite and Fe-Ti oxide minerals. This

fact suggests a close relation of post-depositional formation of smectite and U mineralization in a reducing environment (Komuro, 1991).

Sample Nos. 7, 8, 9 and 12 are from Kanyemba deposit, Zimbabwe, Africa. This deposit is embedded in sandstones in the uppermost part of the Pebbly Arkose Member (Jurassic) and forms some flat-lying ore bodies concordant with the sandstone bedding (Komuro et al., 1989). Oxidized type ores with carnotite are distributed near the surface and the reduced type ores mainly with pitchblende and coffinite are present in the deeper part in well-sorted coarse to medium-grained sandstones consisting of quartz, feldspars and hydromica minerals. The sandstones contain small amounts of carbonaceous materials which fill the interstices of the detrital grains. The detrital quartz and feldspar grains are highly corroded and they float in hydromica minerals associated with coffinite, pitchblende and pyrite. Sutured contact of some floating quartz grains suggests that the formation of hydromica minerals, associated with U mineralization, had occurred after some compaction of host sandstones (Komuro et al., 1989). Vanadium is also found to be associated with hydromica and can be considered to exist in some cases as V-mica mineral (roscoelite) (Suzuki et al., 1990). These mineral paragenesis and textures suggest that U mineralization associated with V has occurred after diagenetic consolidation of sandstones to some extent. This genetic model is quite similar to that of Grants U region, New Mexico, U.S.A. where U-humate is a main controlling factor (Komuro et al., 1992b in prep.).

Sample No.4 is from Key Lake deposit, Saskatchewan, Canada which is considered to be an unconformity-vein type U deposit in the Middle Proterozoic Athabaska Sandstones resting on the Archaean granitic basement. U along with Ni mineralization (pitchblende, coffinite and Ni sulfides and arsenides) occurs in a brecciated and mylonized fault zone and is associated with kaolinization and, to a lesser extent, Fe-rich chlorite. The age of U minerals varies widely from 1228 Ma to 200 Ma after the deposition of the Athabaska Sandstone (Maynard, 1983).

Sample No.1 is from Kurayoshi Mine, Tottori, Japan and represent hydrothermal smectite-quartz veins associated with uranium minerals and sulfides in Tottori granite (Sasada et al., 1979). The K-Ar age of this granite has been determined to be about 61-63 Ma (Shibata and Yamada, 1965; Kawano and Ueda, 1966).

Sample No. 5 is from Bakouma, Central Africa and represents U-rich altered rocks associated with apatite. These apatite beds are in the Tertiary M'Paton Formation consisting of apatite, clay minerals with some pyrite and organic matter. This formation is unconformably lying on the Mouka-Oudda sandstones (Cretaceous?) which rests unconformably on the Precambrian Fouroumbala (crystalline and siliceous rocks) and Bakouma (glacial deposits and dolomite) Formations.

## 3.Analytical Methods

### 3.1 U analyses

The rock samples were first powdered to about 350 mesh-under size (45 μm). These powders mounted in a container were measured for their β and γ-ray radioactivity (counts per minutes) for 5 minutes by means of a Geiger-Muller surveymeter Aloka model JDC-163.

The same rock powders were compressed into pellets of 15 mm in diameter. The bulk U contents of these sample pellets were measured by using a X-ray fluorescence analyzer Rigaku model 3070. U-containing rock powders previously determined for their U contents by a conventional wet chemical analysis were used as standards. These data are tabulated in Table 1.

### 3.2 XRD, UV-VIS-NIR and color analyses

The powdered bulk rock samples are analyzed by X-ray diffractometry (XRD) in order to determine their mineralogical compositions. A Rigaku Rota Flex and Geigerflex X-ray powder diffractometers with CuKα radiation were used. The operating conditions were 80 kV and 40 mA for bulk analyses and 50 kV and 35mA for clay analyses.

The bulk sample powders are then analyzed by diffuse reflectance ultraviolet - visible - near infrared (UV-VIS-NIR) spectroscopy for the wavelength region of 250 to 1500 nm. A spectrophotometer Hitachi U-3410 with a 60 mmϕ integrating sphere was employed to take spectra directly on about 20 to 200 mg of the sample powders placed in containers with quartz windows. Alumina powder was used as a standard white powder to obtain reference spectra. Some sample powders were also measured by a spectrophotometer Minolta CM-2002 for approximate diffuse reflectance spectra with 10 nm steps of wavelength resolution. The detail description of this apparatus is almost the same as for Minolta CM-1000 given in Nakashima et al.(1992) in this volume.

Color measurement has been conducted on these sample powders by using Colorimeters Minolta CR-200 and CM-2002 based on the method already given in Nagano and Nakashima (1989) and Nagao and Nakashima (1991). Detailed description of the method is also presented in Nakashima et al.(1992) in this volume. The colors of sample powders are presented in the second CIE 1976 color space in terms of L*, a* and b* values. L* is psychometric lightness and corresponds to black (L*=0) and white (L*=100). a* and b* are psychometric chromaticness. Plus values of a* correspond to red color, minus ones to green. Plus b* values corresponds to yellow, minus ones to blue.

In order to separate clayish materials (size inferior to 2 μm) from other minerals, the samples have been treated by centrifugation. The sample powders are put in tubes with distilled water and then centrifuged successively at 1000 rpm for 3.5 minutes and 3000 rpm for 40 minutes. Nearly no supernanant particles (inferior to 0.2 μm) were noticeable. The products of centrifugation (particles between 0.2 and 2 μm) are dried in air at a room temperature. These clayish powders were analyzed by XRD for the identification of clay minerals (Table 1).

### 3.3 Electron Spin Resonance (ESR) spectroscopy

The fine particle powders obtained by the above separations were used to take ESR spectra. 10 to 60 mg of powders were put in silica tubes of 4 mm in diameter and then put in a cavity of ESR spectrometer JEOL RE2X. The ESR spectra are obtained at the modulation frequency of 100 kHz and the time constant is of 0.03 seconds. Saturation of centers has been studied from 0.1 to 200mW. The used power for routine spectra was 1 mW. The total ESR spectra were recorded between 800 to 3800 Gauss and the zoomed spectra on radiation centers were recorded from 3050 to 3550 Gauss.

### 3.4 Cathodoluminescence (CL) measurement

Polished thin sections of rock samples were prepared for their petrographic observation under a polarizing microscope, cathodoluminescence examination and compositional mapping under an electron microprobe.

Cathodoluminescence (CL) examination was carried out with a Nuclide ELM-3R Luminoscope mounted in a Nikon Optiphoto 2-Pol microscope. The operating conditions were: a electron beam energy of 10-14 kV, a sample beam current of 300-500 μA, an incident spot diameter of 5-10 mm and an 50 millitorr of air pressure inside the sample chamber. Photomicrographs of emitted CL were taken on the microscope using KONIKA GX 3200 color film of 3200 ASA with 30-120 seconds of exposure time (depending on the CL intensity and on the objective lenses).

Compositional mapping of the same thin section was conducted by means of a computer-controlled supermicroprobe JEOL-8621. The operating conditions were: an accelerating voltage of 15 kV, a probe current of 2 x $10^{-5}$A, a beam diameter of 1-2 μm and counting time of 30 milliseconds.

## 4. Results

### 4.1 XRD and UV-VIS-NIR data

The mineralogical compositions determined by XRD for bulk rock powders are quartz, feldspars and clay minerals (kaolinite, halloysite, chlorite, smectite, illite, interstratified illite-smectite and interstratified kaolinite-smectite) with sometimes muscovite, gypsum, calcite, galena and amphiboles. These data are summarized in Table 1.

Some typical diffuse reflectance UV-VIS-NIR spectra measured on the same sample powders are presented in Fig.1. The results indicate that the absorption band at around 1400 nm (overtone of OH) can be taken as the semi-quantitative indicator of the amount of hydrated phases such as clays. These data are generally consistent with the results of XRD. The absorption bands observed in the visible region are weak bands as shoulders on UV tails but sometimes become recognizable. The band at around 360, 440, 500 and 600 nm can be attributed to $Fe^{3+}$ mainly in octahedral sites of crystal structures (Schoonheydt, 1982; Manceau, 1990), those around 500

and 640 nm to goethite (α-FeOOH)-like material and the large shoulder around 550 nm accompanied by a broad band at 900 nm to hematite ($Fe_2O_3$)(Fig.1). Bands around 960 and 1150 nm can also be recognized for some smectites and these bands can be attributed to $Fe^{2+}$ in octahedral sites (Manceau, 1990) (Fig.1). These data are generally consistent with the presence of $Fe^{3+}$ and Fe oxyhydroxides signals in Electron Spin Resonance (ESR) spectra (Table 1, see also Fig.4a).

Approximate diffuse reflectance spectra for some subsamples from Yotsugi deposit, Ningyo-toge mine, Japan are presented in Fig.2. Despite the rough spectral resolution (10 nm), two main bands can be observed. The broad band around 500 nm is considered to be due to Fe hydroxides. The weak band at 425 nm can possibly be due to the presence of uranyl species (Nakashima, 1991a,b and c). In fact, XRD data on some of these subsamples indicate the presence of uranyl minerals such as metaautunite.

These visible spectra data can be more easily shown graphically by the color data for these samples plotted in an a*-b* diagram (Fig.3). The colors of samples are generally situated near a*=0 axis with varying values of b* (yellow) from 7 to 30. The presence of $Fe^{2+}$ in clays (eg. sample No.1, see also Fig.1) gives minus values of a* (green). The yellowish colors of some of the samples (eg. sample Nos. 2, 10 and 4, see also Fig.1) can be explained by the presence of $Fe^{3+}$ in clays, while the presence of Fe hydroxides contribute to the increase in both b* and a* values (see goethite trend in Fig.3 after Nagano and Nakashima, 1989). The color of sample No.5 with 550 nm visible band (attributed to hematite, Fig.1) is characterized by the high a* (red) value. However, the data point is not on the proposed trend of hematite-containing materials (Nagano and Nakashima, 1989). This fact can be understood by the presence of $Fe^{3+}$ in clays giving a high b* (yellow) value. Much more higher b* values than other samples are observed for the subsamples from the conglomerate matrix of Yotsugi deposit (Y series samples in Fig.3). This high yellowfulness can be attributed to the presence of uranyl species indicated by XRD and VIS data. This Fig.3 is hence useful to classify the samples by the different contributions of color centers.

XRD analyses on fine particle fractions between 0.2 and 2 μm indicate the presence of kaolinite for Sample Nos. 5 and 4. Halloysite was found present for sample No.10. Smectite was identified for Sample Nos. 14, 9 and 1. Interstratified (mixed layer) clay minerals of kaolinite-smectite series were found for Sample Nos. 2 and 11 and those of illite-smectite series were present for Sample Nos. 7, 8 and 12 (Kanyemba).

### 4.2 ESR data on radiation damage centers in clays

Some total ESR spectra on clayish fractions of rock samples from U deposits are presented in Fig.4. Various ESR signals were observed and they can be classified as follows (see also Table 1).

The signals due to $Fe^{3+}$ in octahedral sites of clay minerals with an ESR parameter g value of about 4.2 can be recognized in sample Nos.1, 10, 2,

3, 6, 5 and 4 (Fig.4). Sample Nos. 2 and 10 clearly contain broad signals around 2300 Gauss due to Fe oxyhydroxides (Fig.4b and c). We have noticed also the signals of paramagnetic metal species such as $Mn^{2+}$ (6 hyperfine lines due to the interaction of unpaired electron with nuclear spin with a splitting constant of 90-100 gauss, centered near g=2.0) for sample Nos.10 and 13 (Fig.4c), $Cu^{2+}$ (asymmetric signal with four-line hyperfine structure) for sample No. 4 (Fig.4d) and $V^{4+}$ (centered near g=2.0, with 2 groups of hyperfine structures related to g// and g⊥) for sample Nos.12 and 5 (Fig.4e).

The same type of radiation center signals as those of kaolinite (Clozel, 1991) have been observed for 4 samples, Nos.10, 2, 5 and 4. These signals appear between 3200-3400 Gauss (Fig.4). The main component of the signals of sample Nos.2 and 10 (Fig.4b, c) is considered to be mainly due to the "A center" which is the most stable center among three different ones in kaolinite (A, A' and B centers) (example of signal: sample No.10, Fig.5). The shape of the signals sometimes appears to be similar to signals of hydrothermal kaolinite without actual association with uranium (Clozel, 1991).

The intensity of these defect center signals were calculated based on the peak heights around g=2.0 after the subtraction of signals due to paramagnetic metals and presented in Table 1. These values in kaolinite-like clays can be taken as approximate indicators of degrees of radiation damages and so that the degrees of contact with radionuclides.

For the sample No.5 an initial treatment of data was necessary because of the overlapped signal of vanadium. Knowing a pure signal of vanadium without defect center signal (sample No.12), a spectral substraction can be performed to obtain an ESR spectrum free of vanadium signals. The resulting spectrum indicate much more pronounced contributions of A and A' centers. The presence of A' center in this sample No.5 suggests a close contact of kaolinite with radionuclides.

The decomposition of sample No.4 signal was not possible because of the overlapping of Cu signals and only an approximate intensity of total signal was determined.

The samples showing the kaolinite-like radiation damage centers contain actually kaolinite for samples Nos. 2, 5 and 4 identified by XRD analyses (Table 1). However, sample No.10 have only halloysite as clay minerals and show the kaolinite-like radiation centers. All other samples containing illite-smectite series do not exhibit ESR signals due to radiation centers.

### 4.3 Cathodoluminescence (CL) data on radiation damages in quartz

The results of radiation damage rims examined by CL are summarized in Tables 1 and 2. The damage rims are recognized in samples Nos. 2 and 15 (Ningyo-toge mine), Nos. 13 and 6 (Tono mine), Nos. 7, 8 and 12 (Kanyemba deposit) and No. 4 (Key Lake deposit), and they are not

recognizable for sample Nos. 1 (Kurayoshi mine),10 (Ningyo-toge Mine), 3 and 11 (Tono mine).

In fine grained samples such as sample No.14 (Tono), No.9 (Kanyemba) and No.5 (Bakouma), the recognition of these rims is difficult because the sizes of grains are too small.

Radiation damage rims in quartz grains in these samples are generally brownish orange under CL observation, in contrast to usual reddish brown CL color of normal quartz grains (Table 2). For some of the samples from Kanyemba, grayish blue rims can also be recognized for some bluish brown quartz grains (Plate 1). These grayish blue rims can be recognized as two occurrences. One is as an inner part of a zonal structure where the orange rim is at the surface of bluish gray quartz grains (Plate 1b). The other is the presence of grayish blue rims without orange ones (Plate 1a). The difference of the two different colors of rims is somewhat difficult to be observed because of the difference of CL color of original quartz grains (reddish brown vs. grayish-blue) (Zingernagel, 1978).

The width of the rims are generally in the range of 25-30 μm. In some cases, concentric rings of different colors are visible at several intervals especially around minute inclusions such as Zircon and Fe-Ti oxides which are considered to be acting as point sources of irradiation (Plate 1c). In sample 12, poorly developed rims are generally observed with a width of about 20 μm at the quartz surface, but their CL color has a low contrast. On the other hand, in this sample, well developed rims exist around zircon, Fe-Ti oxides and vanadiferous clays.

The distribution of rims in these samples can be classified into two groups (Table 2). In the first group including sample Nos. 15, 13, 6, 8 and 4, the rims are recognized in almost all quartz grains throughout the thin section samples (Plates.1a, 1b, 2, 3 and 5). For the second group including sample Nos. 2 and 7, the rims are observed in quartz grains which are in contact with specific minerals. Sample No. 2 is characterized by the rims distributed around veins containing metaautunite (Plate 4), while sample No.7 has the rims around zircon, Fe-Ti oxides and vanadiferous clays. The distribution of radionuclides is disperse in the first group, whereas their distribution is concentrated in specific minerals for the second group.

## 5. Discussion

### 5.1 Radiation Centers in clays by ESR

The presence of kaolinite-like radiation centers in some of the samples (Nos. 2: Ningyo-toge, 5: Bakouma and 4: Key Lake) containing kaolinite and uranium from the different U deposits in the world is consistent with our hypothesis that this type of radiation damages can be widespread in various types of U deposits (Clozel, 1991). These samples are from oxidized or altered type of U ores and these alteration processes have resulted in the formation of kaolin group minerals. Though these samples have generally high U contents (>0.1 wt % as $U_3O_8$), they do not have a direct positive

correlation with the intensity of radiation centers (Table 1).

We will recall here the previous results on three different radiation centers in kaolinite (Clozel, 1991). The A center in kaolinite has been considered to be due to a hole trapped on O (pointing from the tetrahedra to the octahedral layer) bonding one part to Si of a $SiO_4$ tetrahedra and other parts to $Al^{3+}$ and $Al^{3+}$ (or substituting $Mg^{2+}$) of an octahedral layer. This center is related to the damage caused by an ionization upon irradiation. This A center is the most stable one and is considered to conserve a memory of irradiation for the period superior to 1 million of years (1 Ma) at 80 °C. A' center is a hole trapped on O oriented to the tetrahedral layer plain and is stable probably for the period between one hundred and several thousands of years at around 25 °C and several years at 80 °C and is related to the atom displacement associated with α-recoil. B center is a hole trapped on O between two Al in the octahedral layer and is the most unstable one. This center have its stability for the period of 10 to 100 years at around 25 °C and several months at 80 °C so that is an indicator of a recent irradiation.

The radiation damages in kaolin group minerals in the present study should have been formed by a close contact with radionuclides for certain period of time. Even if the radionuclides have recently escaped from the site, the stable damage signatures could have been conserved. The actual U content do not necessarily correlate with the radiation centers. The intensity of the radiation center signals is rather a measure of paleo-presence of radionuclides for a relatively long period. For instance, sample No.4 from Key Lake, Canada have a wide range of ages of U minerals from 1228 to 200 Ma and is considered to have a long period of U contact with kaolinite which gives a high intensity of radiation damage signals (Table 1; ESR signal intensity 14 U.A).

Sample No.5 from Bakouma, Africa (Table 1; 9 U.A) seemed to contain significant components of unstable A' and B centers besides A center. A recent contact of radionuclides with kaolinite can be supposed.

Clay mineral identified for Sample No.2 from Ningyo-toge is interstratified kaolinite-smectite. This sample contain relatively high U content (1.28 wt% $U_3O_8$). The kaolinite-like A center (most stable one) is considered to be a main component of ESR signals (Table 1; 4 U.A). Since all the other samples containing smectite-like components (such as Tono Mine and Kanyemba) do not exhibit radiation damage signals, the origin of this stable damage is considered to be due to the presence of kaolinite structure together with its close contact with high concentration of U.

The kaolinite-like radiation centers were observed on halloysite of sample No.10 (Table 1). This result can be understood by the structural similarity of halloysite to kaolinite. Since halloysite has the same structural unit as kaolinite with much more incorporated waters between its layers, the same origin of defect centers as kaolinite can be expected for halloysite. The sample No.10 has only low content of U (0.02 wt% $U_3O_8$) but exhibit the kaolinite-like radiation centers with a high signal intensity (Table 1; 8

U.A). This fact suggests a hypothesis that water in the kaolinite structure can favor the formation of radiation damage centers. Halloysite can be hence much more sensitive to radiation damages than kaolinite. The other possibility of the origin of high damage signals in this sample is the following. The initial reduced type orebody has been altered by groundwater leaching of U to form halloysite in rock matrix. Halloysite is considered to have been adjacent to fissures for certain period during the repetitive U removal. Halloysite have hence experienced much irradiation in sample No.10. In any case, the origin of significant radiation damages recorded in this halloysite without actual high U content should be studied further for the better understanding of radiation centers in halloysite and their geochemical implications.

The XRD analyses on the fine particle fractions of the other rock samples indicate the presence of other clay minerals than kaolinite such as smectite and illite. Though some of these samples contain high concentration of U (Nos.1, 11, 13 and 8 > 0.1 wt% $U_3O_8$, Table1), these clay minerals do not exhibit radiation damage centers. It should be noted that the presence of ESR signal of Fe can mask the defect center signals.

Smectites and illite have similar structural portions as kaolinite in some parts of their structures. However, they do not seem to exhibit the radiation damages. The first structural reason of this instability of radiation defects for smectites and illites can be attributed to the easy charge compensation of defective layers in these minerals. The second reason can be originated from the presence of Fe in these minerals. The poisoning of Fe for the defect centers can be explained tentatively by the fact that the lack of positive charge, which is an initial origin of the formation of an O hole center, can be compensated by the oxidation of $Fe^{2+}$ to $Fe^{3+}$.

### 5.2 Radiation damage rims in quartz by CL

The development of the radiation damage rims observed for quartz grains of the rock samples can be roughly correlated with the U contents and radioactive counts on the rock powders (Fig.6a,b). The samples with higher U contents than 1 wt% $U_3O_8$ have always these rims, while those with lower U content do not exhibit them except for the Kanyemba samples.

The age of U mineralization should also be taken into account, since the development of the rims is a function of contact time between radionuclides and quartz. The samples from Kanyemba (Jurassic) have one or two orders of magnitude lower U content than Ningyo-toge and Tono (Miocene) samples, but they have well-developed rims. This fact can be understood by the longer contact (maximum of about 200 Ma) for Kanyemba than for Ningyo-toge and Tono (maximum of about 20 Ma).

The origin of these CL rims has been hypothesized by Owen (1988) to be due to damages created by α particles emitted by radionuclides. He has calculated penetration distance of α particles in quartz to be about 13 to 36 μm by using various energies of α-particles from 4.2 to 7.7 MeV emitted by uranium series nuclides. The rim widths generally observed in our

samples are within this range.

Kanyemba quartz grains exhibit grayish blue CL rims beside orange ones. Our preliminary data on CL spectra on these samples indicate two major CL emission bands around 470 nm and 610 nm. The CL emission on the rims of quartz grains seems to be richer in the reddish component (610 nm band) than the inner parts. The blue CL band around 470 nm can correspond to the E′ center associated with an oxygen vacancy in Si-O-Si (Walker, 1985). The red one around 610 nm can correspond to the oxygen-associated hole center (OHC) on non-bridging oxygens which has been known to be induced by irradiation of neutrons or γ-rays. This OHC center is considered to be associated with Si-OH, since this center is prevailing in silica with a high OH content (Walker, 1985). The distribution of the red CL rims at the surface of quartz grains in this study might reflect the Si-OH related OHC centers created at hydrated surface layers of quartz.

We have conducted preliminary ESR measurement on these quartz grains separated from the sandstone matrix from Kanyemba. The resulting ESR spectra indicate the presence of E′ center. Approximate integrated intensities of E′ center component seem to remain in the same order of magnitude for the matrix U contents of 4.59, 0.09 and 0.02 wt%. The blue CL band cannot therefore be directly correlated with the actual U contents, while the red CL rims can be much more directly related to them.

The origin of zonal structure of blue and red CL rims in some quartz grains of Kanyemba (Plate 1b) can be tentatively explained by the less stable nature of the red center. The red and blue centers are considered to be created simultaneously by the contact with U. If significant amount of U has escaped from the matrix adjacent to the quartz grains, the unstable red centers will gradually be recovered from the inner part of the grains and so that the blue center will become recognizable. This explanation is only a working hypothesis and further data are needed to clarify this hypothesis.

In these kaolinite-free samples, quartz grains are the most effective damage records and so that much more detailed studies will be pursued.

## 6. Conclusions

Rock samples from different world U deposits in sedimentary rocks have been studied by Electron Spin Resonance (ESR) spectroscopy and Cathodoluminescence (CL) measurement in order to characterize radiation damage centers in clays and quartz.

The presence of kaolinite-like radiation centers in ESR spectra in some of the samples containing kaolin group minerals suggest that these type of radiation damages can be widespread in altered or oxidized type of uranium deposits. The main component of the signals is considered to be due to the "A center" which is the most stable center among three different ones in kaolinite (A, A′ and B). Though these samples have generally high U contents (>0.1 wt % as $U_3O_8$), they do not have a direct positive correlation

with the intensity of radiation centers. This intensity is rather a measure of paleo-presence of radionuclides for a relatively long period. For instance, sample No.4 from Key Lake, Canada have a wide range of ages of U minerals from 1228 to 200 Ma and is considered to have a long period of U contact with kaolinite which gives a high intensity of radiation damage signals.

Sample No.5 from Bakouma, Africa seemed to contain significant components of unstable A' center besides A center. A close contact of radionuclides with kaolinite can be supposed.

The kaolinite-like radiation centers were observed on halloysite of sample No.10 having only low content of U (0.02 wt% $U_3O_8$) . This result can be understood by the structural similarity of halloysite to kaolinite and the possible favoring of defect formation by the presence of water.

The other clay minerals than kaolinite such as smectite and illite present in some of the samples do not exhibit radiation damage centers even with high concentration of U (Nos.1, 11, 13 and 8 > 0.1 wt% $U_3O_8$). This instability of radiation defects for smectites and illites can be attributed hypothetically to the easy rearrangement of their structures for the charge compensation of defective layers or the presence of $Fe^{2+}$-$Fe^{3+}$ pair in these minerals.

CL measurement on quartz grains indicated the presence of radiation damage rims for the samples having high U contents (> 1 wt% $U_3O_8$). These rims can also be recognized for older samples (Kanyemba U deposit) with low U concentration. This fact can be understood by the longer contact (maximum of about 200 Ma) for Kanyemba than for Ningyo-toge and Tono (maximum of about 20 Ma).

Radiation damage rims in quartz grains in these samples are generally brownish orange under CL observation. For some of samples from Kanyemba and Key Lake deposit, grayish blue rims can also be recognized for some bluish brown quartz grains as an inner part of a zonal structure with the orange rims at the surface of quartz grains or as grayish blue rims without orange ones. The width of the rims are generally in the range of 25-30 μm in accordance with the hypothesized penetration depth of α particles of about 13 to 36 μm (Owen, 1988).

The distribution of rims in these samples can be classified into two groups. In the first group including sample Nos. 15, 13, 6, 8, 12 and 4, the rims are recognized in almost all quartz grains throughout the thin section samples. For the second group including sample Nos. 2 and 7, the rims are observed in quartz grains which are in contact with specific U-bearing minerals.

Kanyemba quartz grains exhibit grayish blue CL rims beside brownish orange ones. The blue CL emission around 470 nm can correspond to the E' center (Walker, 1985) without direct correlation with actual U contents. The red CL emission around 610 nm can correspond to the oxygen-associated hole center (OHC) on non-bridging oxygens forming OH bonds which has been known to be induced by irradiation of neutrons or γ-rays (Walker,

1985). These reddish CL rims can be much more directly related to actual U distributions.

Although some of the samples could not be determined systematically by both methods, the samples having high U content (>1 wt% $U_3O_8$), kaolins and quartz (Nos. 2 and 4) exhibit consistent ESR and CL damage records (Fig.6a).

When kaolin group clays are present, they can preserve radiation damage ESR signals for U contents as low as 0.02 wt% $U_3O_8$ (for a halloysite bearing young sample), while CL rims can be observed for a relatively old quartz grains with until 0.02 wt% $U_3O_8$ of matrix U contents. Kaolinite can be a sensitive indicator of relatively young contacts with U, while quartz grains can record a long contact with U. In kaolinite-free samples, quartz grains are the most effective damage records.

Much more systematic studies are needed in order to clarify the relation between the radiation damage centers and the actual U concentration and also on the possibility of indicators of paleo-presence of radionuclides. For further detailed studies, extensive analyses of ESR spectra on quartz, CL spectra measurement on quartz and thermoluminescence experiments under a microscope by using a newly developed visible microspectrometer (Nakashima et al., 1992) combined with a cooling-heating stage for both quartz and clays will be pursued.

## Acknowledgments

The authors would like to thank Dr. M. Senoo of Japan Atomic Energy Research Institute (JAERI), Dr. M. Yamakawa and Mr. K. Otomura of Power Reactor and Nuclear Fuel Development Corporation (PNC) for their support of this work. Mr. Y. Otsuka and Mr. M. Yamamoto of PNC are gratefully acknowledged for their useful assistance in sample preparation and analyses. A major part of this work has been conducted at JAERI by one of the authors (B.C.) during her post-Doctoral stay as Research Fellow.

## References

Calas, G. (1988): Electron Paramagnetic Resonance. In *"Spectroscopic Methods in Mineralogy and Geochemistry"* (ed. Hawthorne, F.C.), Mineral. Soc. Amer., Washington, D.C. p.513-571.

Clozel, B. (1991): Etude des défauts paramagnéniques induits par irradiation dans les kaolinites - Approche expérimentale et implications géochimiques -. Doctoral Thesis, University of Paris VII.

Doi, K. and Hirono, S. (1990): Behavior of uranium migration in epigenetic uranium ore deposits with reference to radioactive waste isolation in geologic media. *Waste Management*, **10**, 275-284.

Doi, K., Hirono, S. and Sakamaki, Y. (1975): Uranium mineralization by groundwater in sedimentary rocks, Japan. *Econ. Geol.*, **70**, 628-646.

Hall, P.L. (1980a): The application of electron spin resonance spectroscopy

to studies of clay minerals: I. isomorphous substitutions and external surface properties. *Clay Minerals*, 15, 321-335.
Hall, P.L. (1980b): The application of electron spin resonance spectroscopy to studies of clay minerals: II. Interlamellar complex-structure, dynamics and reactions. isomorphous substitutions and external surface properties. *Clay Minerals*, 15, 337-349.
Ildefonse, Ph., Muller, J-P., Clozel, B. and Calas, G. (1990): Study of two alteration systems as natural analogues for radionuclide release and migration. *Eng.Geol.* **29**, 413-439.
Ildefonse, Ph., Muller, J-P., Clozel, B. and Calas, G. (1991): Record of past contact between altered rocks and radioactive solutions through radiation-induced defects in kaolinite. *Scientific Basis for Nuclear Waste Management XIV* (MRS Symp. Proc. Vol.212), 749-756.
Kawano, Y. and Ueda, Y. (1966): K-A dating on the igneous rocks in Japan (V) - granitic rocks in southwestern Japan -. *Jour. Japan. Assoc. Mineral. Petrol. & Econ. Geol.* , **56**, 191-211 (in Japanese).
Komuro, K.(1991): Environment and mechanisms of uranium deposition in Tono uranium deposit. PNC TN1410 91-079, 325-336 (in Japanese).
Komuro, K., Suzuki, S., Ohtsuka, Y., Yamamoto, M. and Koyama, K. (1989): Uranium occurrences in the Kanyemba deposit, Zimbabwe. Abstracts with Programs, Joint Annual Meetings of the Society of Mining Geologists of Japan, the Japanese Association of Mineralogists, Petrologists and Economic Geologists of Japan and the Mineralogical Society of Japan (Niigata), 169 (in Japanese).
Komuro, K., Yamamoto, M., Suzuki, S., Nohara, T. and Takeda, S.(1990): Uranium occurrences in the Tsukiyoshi ore deposit, Tono district. *Mining Geol.*, **40**, 44 (in Japanese).
Komuro, K., Ohtsuka, Y. and Yamamoto, M. (1991a): Uranium occurrences in the Tsukiyoshi ore deposit, Tono district (part 2) - Uranium occurrences associated with Fe-Ti oxides and heulandite -. *Mining Geol.*, **41**, 177-178 (in Japanese).
Komuro, K., Ohtsuka, Y. and Yamamoto, M. (1992a in prep.): Fossil radiation damage rims in quartz from some uranium mineralized area.
Komuro, K., Ohtsuka, Y., Yamamoto, M. and Fukushima, T. (1992b in prep.): Uranium mineralization of the Kanyemba-1 deposit, Zimbabwe.
Manceau, A. (1990): Spectroscopie Optique. In "Matériaux Argileux", Soc. Fr. Mineral. Crist., Paris, p.57-74.
Marfunin, A.S. (1979): *Spectroscopy, Luminescence and Radiation Centers in Minerals.* Springer Verlag, Berlin, 352pp.
Maynard J.B. (1983): Uranium, In"Geochemistry of Sedimentary Ore Deposits", Chapter 6, Springer-Verlag, New York, p.147-180.
Meunier, J-D., Sellier, E. and Pagel, M. (1990): Radiation-damage rims in quartz from uranium-bearing sandstones. *Jour. Sediment. Petrol.* **60**, 53-58.
Muller, J.P. and Calas, G. (1989): Tracing kaolinites through their defect centers: kaolinite paragenesis in a laterite (Cameroon). *Econ. Geol.* **84**,

694-707.
Muller, J-P., Clozel, B., Ildefonse, P. and Calas, G. (1992): Radiation-induced defects in kaolinites : Indirect assessment of radionuclide migration in the geosphere. accepted to *Applied Geochemistry*.
Nakashima, S. (1990): Analysis and prediction of geochemical dynamic processes near the earth's surface. *J. Mineral. Soc. Japan*, **19**, p.289-293 (in Japanese).
Nakashima, S. (1991a): Fourier-transform multichannel visible microspectroscopy of rocks. *Hitachi Scientific Instruments News*, **34**(2), 3278-3284 (in Japanese).
Nakashima, S. (1991b): Radionuclide fixation mechanisms in rocks. Proc. 3rd Intl. Symp. on Advanced Nuclear Energy Research *"Global Environment and Nuclear Energy"*, 159-166, JAERI, Tokai, Japan.
Nakashima, S. (1991c): Earth's resources and environment - an example of the global geochemical cycle of uranium-. *J.Mineral.Soc.Japan*, **20**, 233-241 (in Japanese).
Nakashima, S. (1992a, in press): Complexation and reduction of uranium by lignite. *Science of the Total Environment* ##, ###-###.
Nakashima, S. (1992b, submitted): Kinetics and thermodynamics of uranium reduction by natural and simple organic matter. submitted to *Organic Geochemistry* .
Nakashima, S., Disnar, J-R., Perruchot, A. and Trichet, J. (1984): Experimental study of mechanisms of fixation and reduction of uranium by sedimentary organic matter under diagenetic or hydrothermal conditions.*Geochim. Cosmochim. Acta*, **48**, p.2321-2329.
Nakashima, S., Disnar, J-R., Perruchot, A. and Trichet, J. (1987): Fixation et réduction de l'uranium par les matières organiques naturelles: mécanismes et aspects cinétique. *Bull. Mineral.* **110**, p.227-234 F.
Nakashima, S.. Miyagi, S., Nakata, E., Sasaki, H., Nittono, S., Hirano, T., Sato, T. and Hayashi, H. (1992): Color Measurement of Some Natural and Synthetic Minerals - I. in this issue.
Nakashima, S., Miyamoto, M., Zolensky, M., Jin, C., Minorikawa, M., Sunose, M. and Sakuma, K. (1992 in press): Development of infrared and visible microspectroscopy for the in-situ characterization of chondrites and cosmic dust particles. *Grain Formation Workshop XIII*, Grain Formation in the Universe Working Group, ##-##.
Nagano, T. and Nakashima, S. (1989): Study of colors and degree of weathering of granitic rocks by visible diffuse reflectance spectroscopy. *Geochem. J.*, **23**, p.75-83.
Nagao, S. and Nakashima, S. (1991): A convenient method of color measurement of marine sediment by chromameter.*Geochem. J.*, **25**, 187-197.
Owen, M.R. (1988): Radiation-damage halos in quartz. *Geology*, **16**, 529-532.
Sasada, M., Yamada, N., Sakiyama, T. and Ueda, K. (1979): Late

Cretaceous to Paleogene igneous rocks in the Misasa-Okutsu-Yubara area, eastern Chugoku District, southwest Japan. In *"Mesozoic acid igneous activity in Japan"* (ed. Murakami, N.), The Memoirs of Geological Society of Japan, No.17, 19-34.

Schoonheydt, R.A. (1982): Ultraviolet and visible light spectroscopy. In *"Advanced Techniques for Clay Mineral Analysis"* (ed. Fripiat, J.J.), Developments in Sedimentology 34, Elsevier, Amsterdam, p.163-189.

Shibata, K. and Yamada, N. (1965): Potassium-argon ages of the granitic rocks in the vicinity of Ningyo-toge, Chugoku district, west Japan. *Bull. Geol. Surv. Japan*, **16**, 437-442.

Smith, J.V. and Stenstrom, R.C. (1965): Electron-excited luminescence as a petrological tool. *Jour. Geol.*, **73**, 627-635.

Suzuki, S., Komuro, K., Ohtsuka, Y., Yamamoto, M. and Koyama, K. (1990): Alteration haloes around the Kanyemba uranium deposit, Zimbabwe. *Mining Geol.*, **40**, 44-45 (in Japanese).

Walker,G. (1985): Mineralogical applications of luminescence techniques. In *"Chemical Bonding and Spectroscopy in Mineral Chemistry"* (eds. F.J.Berry and D.Vaughan), Chapman and Hall, London, p.103-140.

Zingernagel, U. (1978): Cathodoluminescence of quartz and its application to sandstone petrology. *Contrib. Sedimentology*, **8**, 1-69.

# Table 1. XRD and ESR results of studied samples from different U deposits.

| Sample | Locality | Mode of occurence | Mineral composition by XRD Bulk | <2µm | ESR signal | Wt%$U_3O_8$ (cpm) | CL Rims |
|---|---|---|---|---|---|---|---|
| 1 | Tottori (Japan) Kurayoshi mine Aruki-dani deposit | Clay veins associated with U-minerals and sulfides in granite | Clay mineral Qz | Smectite | None Fe3+ | 0.08 (122) | X |
| | Okoyama(Japan) Ningyo-toge mine Yutsugi deposits | Stratabound Uranium deposits in Tertiary sandstone and conglomerate | | | | | |
| 10 | ditto | (reduced type) | Qz, Kf Clay mineral | Halloysite | Kaol. (8 U.A) Fe3+ Mn | 0.02 (137) | X |
| 2 | ditto | (oxydized type) | Qz, pl, Kf Clay minerals | Interstatified Kaolinite-Smectite | Kaol. (4 U.A) Fe3+ | 1.28 (2430) | O |
| 15 | Nakatsuko deposit | Stratabound U deposit in sandstone and conglomerate (reduced type) | Qz, mi, gy, pl, py | ND | ND | 4.81 (25900) | O |
| | Gifu (Japan) Tono mine Tsukiyoshi deposit | Stratabound Uranium deposits in Tertiary sandstone and conglomerate. | | | | | |
| 3 | ditto non-mineralized | | Qz, pl, Kf,mi Clay minerals | Smectite? | None Fe3+ | 0.003 (30) | X |
| 14 | ditto non-mineralized | mudstone | Pl Clay minerals | Smectite + Chlorite? or Kaolinite? | Nonobs | 0.04 (244) | -- |
| 11 | ditto mineralized | matrix of conglomerate (reduced type) | Ca, pl, qz, Kf, heu Clay minerals | Interstratified Kaolinite-Smectite | Nonobs | 0.13 (437) | X |
| 13 | ditto mineralized | matrix of conglomerate (reduced type) | Ca, qz, pl, Kf Clay minerals | Smectite? Calcite | None Mn (calcite) | 2.24 (9210) | O |
| 6 | N°21 outcrop | sandstone (marine) (reduced type) | Qz, pl, Kf, gy, co am? Clay minerals | Smectite | None Fe3+ | 4.78 (29900) | O |
| | Zimbabwe (Africa) Kanyemba deposit | Stratabound Uranium deposits in Jurassic sandstones | | | | | |
| 7 | ditto non-mineralized | medium sandstone | Qz, pl, Kf, mi Clay minerals | Interstratified Illite-smectite | Nonobs | 0.03 (134) | O |
| 8 | ditto non-mineralized | medium sandstone | Qz, pl, Kf, mi Clay minerals | Interstratified Illite-smectite | Nonobs | 0.12 (348) | O |
| 9 | ditto non-mineralized | fine sandstone | Qz, pl, Kf, mi Clay minerals | Smectite | Nonobs | 0.003 (37) | -- |
| 12 | ditto mineralized | fine sandstone | Qz, pl, Kf, mi Clay minerals | Interstratified Illite-smectite | None V | 0.02 (57) | O |
| 5 | Bakouma (Central Africa) | Uranium associated with apatite bed. altered rock (oxidized type) | Mi, Qz, Kf Clay minerals | Illite Kaolinite | Kaol. (9 U.A) Fe3+ V | 0.18 (1210) | -- |
| 4 | Key Lake (Canada) mineralized | Unconformity type deposits. Altered rock (reduced type) | Qz, ca, ga, sp, pi? Clay minerals | Kaolinite | Kaol. (14 U.A) Fe3+ Cu, V | 1.96 (9120) | O |

*Legend for ESR signal:*

None: No radiation induced centers.
Nonobs: No radiation induced centers can be distinguished from other intense signals.
Kaol. Radiation induced centers of the same type as those observed in kaolinite. (intensity of signal U.A)
Fe3+: Presence of Fe3+ in crystal.
Mn, Cu, V: Presence of paramagnetic metal species such as Mn, Cu and V.
ND: Not determined

*Legend of Mineral composition:*

qz: quartz, pl: plagioclases, Kf: alcali-felsdpar, ca: calcite, mi: mica, pi: pitchblende, co: coffinite, py: pyrite, sp: spharelite, ga: galena, gy:gypsum, am: amphibole, heu: heulandite, ND: not determined.

*Legend for CL rims presence of quartz:*

O: Presence of rims.
X: No rims.
-- : Not possible to determine.

Wt% U3O8 data were obtained by XRF method.
All radioactivity measurements of samples were obtained by GM Survey meter.

Table 2. Cathodoluminescence (CL) results on studied samples from different U deposits.

| No. | Locality | Occurrence of rims on quartz grains | | | CL color of rims(CL color of original quartz) *) |
|---|---|---|---|---|---|
| | | General | Around veins | Around minerals | |
| | (Japan) | | | | |
| 2 | Yotsugi deposits, Ningyo-toge mine, Okayama Pref. | × | metaautunite | | pale-BO(RB) |
| 15 | Nakatuko deposits, Ningyo-toge mine, Okayama Pref. | ◎ | | | pale-BO(RB) |
| 13 | Tsukiyoshi deposits, Tono mine, Gifu Pref. | ◎ | | | pale-BO(RB) |
| 6 | No.21 outcrop, Tono mine, Gifu Pref. | ◎ | | | pale-BO(RB) |
| | (Africa) | | | | |
| 7 | Kanyemba deposit, Zimbabwe. | × | | Zircon<br>Fe-Ti oxides<br>V-clays | BO(RB), BO+Gb(GbB), Gb(bB) |
| 8 | ditto | ◎ | | | BO(RB), BO+Gb(GbB), Gb(bB) |
| 12 | ditto | ○ | | Zircon<br>Fe-Ti oxides<br>V-clays | BO(RB), BO+Gb(GbB), Gb(bB) |
| | (Canada) | | | | |
| 4 | Key Lake | ◎ | | | BO(RB), BO+Gb(GbB), Gb(bB) |

*) BO : brownish orange, Gb:grayish blue, RB:reddish brown, GbB:gray-blueish brown, bB:blueish brown
+ : concentric rims, outside(radionuclides side) color+ inside color

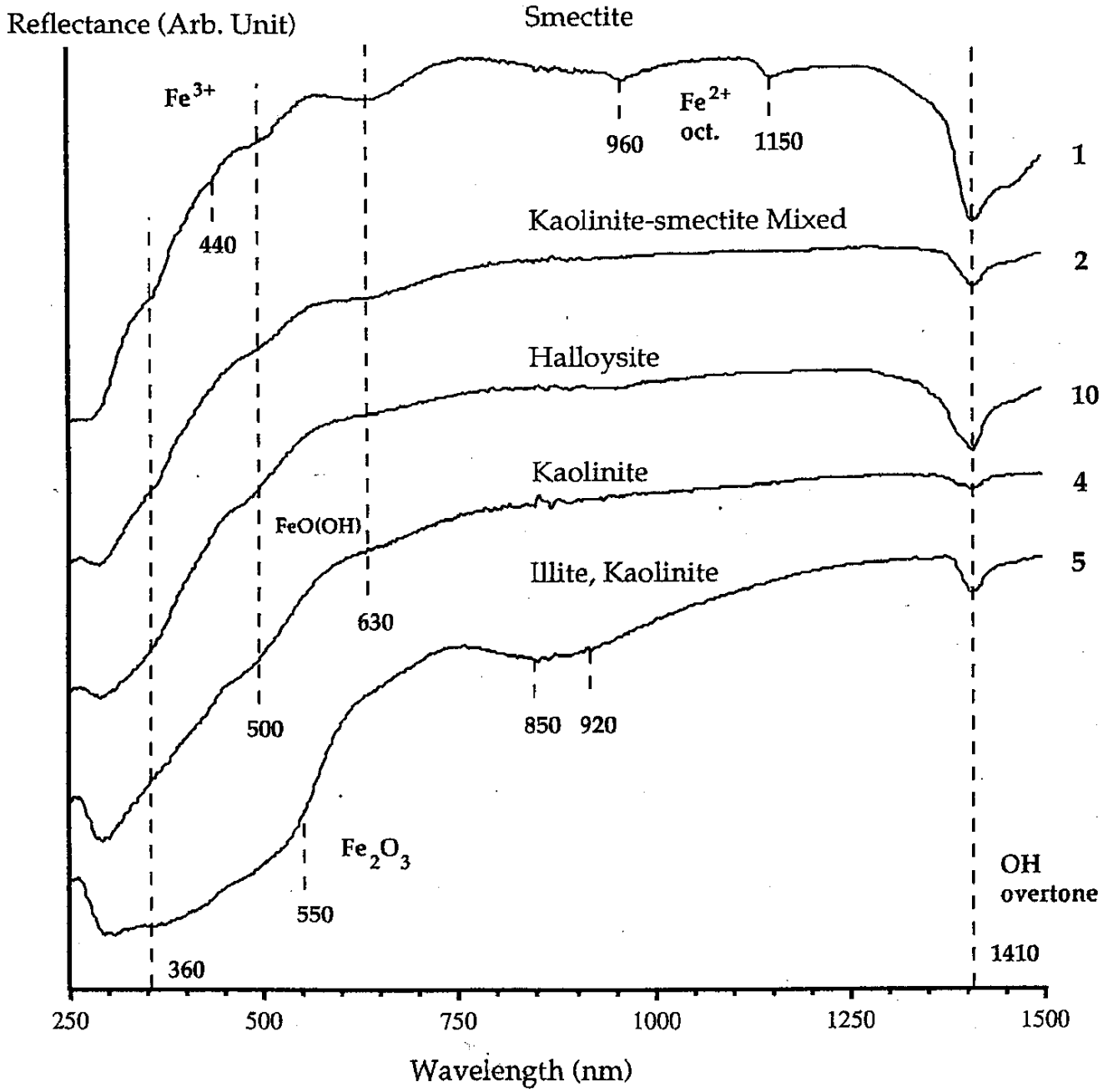


Fig.1 Typical diffuse reflectance UV-VIS-NIR spectra of the bulk sample powders from some U deposits. The bands at 360, 440 and 630 nm can be attributed to $Fe^{3+}$ mainly in octahedral sites of clays, while those at 960 and 1150 nm can be attributable to $Fe^{2+}$ in octahedral sites. The band around 500 nm is considered to be due to Fe hydroxides and those around 550 and 900 nm are indicative of the presence of hematite.

1: sample No.1 containing smectite;
2: sample No.2 containing interstratified kaolinite-smectite;
10: sample No.10 containing halloysite;
4: sample No.4 containing kaolinite;
5: sample No.5 containing illite and kaolinite.

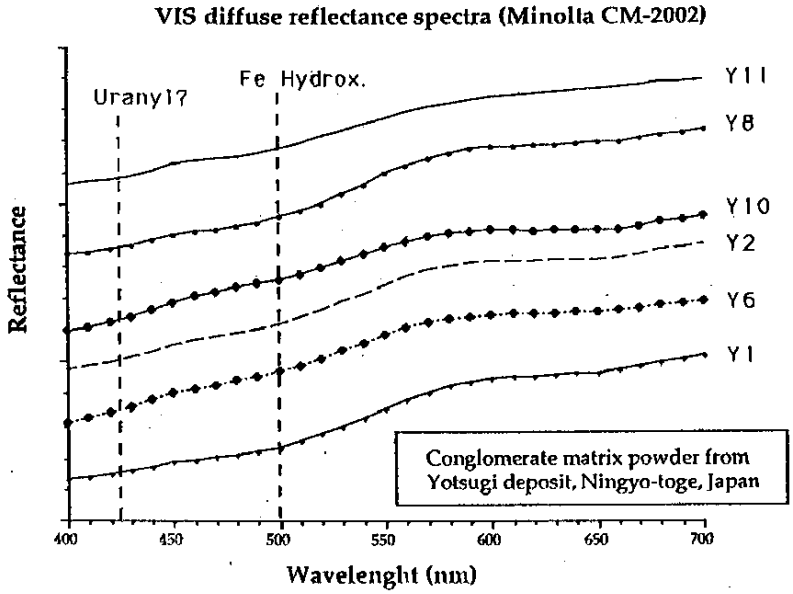


Fig.2 Diffuse reflectance visible spectra obtained by a spectrophotometer Minolta CM-2002 for the conglomerate matrix powders from Yotsugi deposit, Ningyo-toge Mine, Okayama, Japan.

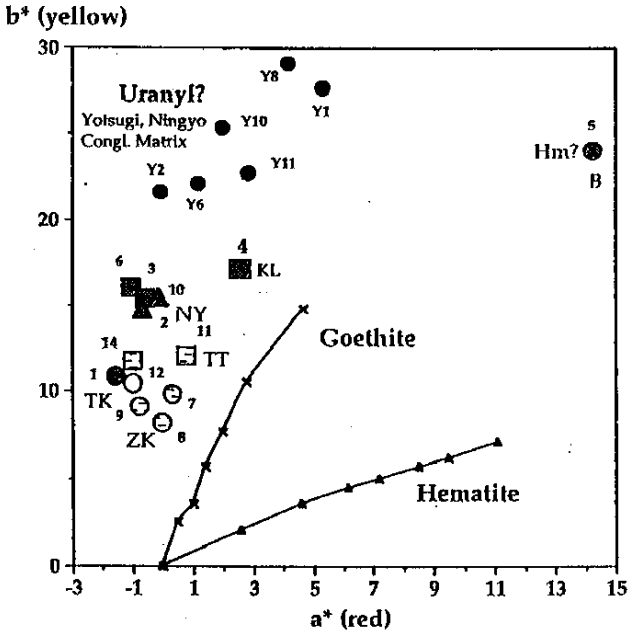


Fig.3 Color of sample powders from some sedimentary U deposits plotted in an a*-b* diagram. The trends for goethite and hematite containing materials (Nagano and Nakashima, 1989) are also presented.
TK: Tottori, Kurayoshi mine; NY: Ningyo-toge, Yotsugi deposit; Y: Matrix powders of conglomerates from Yotsugi deposit; TT: Tono mine, Tsukiyohi deposit; ZK: Zimbabwe, Kanyemba deposit; B: Bakouma; KL: Key Lake. Numbers are the sample numbers indicated in Table 1.
: Presence of $Fe^{3+}$ in octahedral sites of clay indicated by ESR;
: Presence of too much iron to distiguish the sites of iron in minerals;
Hm? : Presence of hematite indicated by VIS spectra;
Uranyl? : Presence of uranyl indicated by VIS spectra.

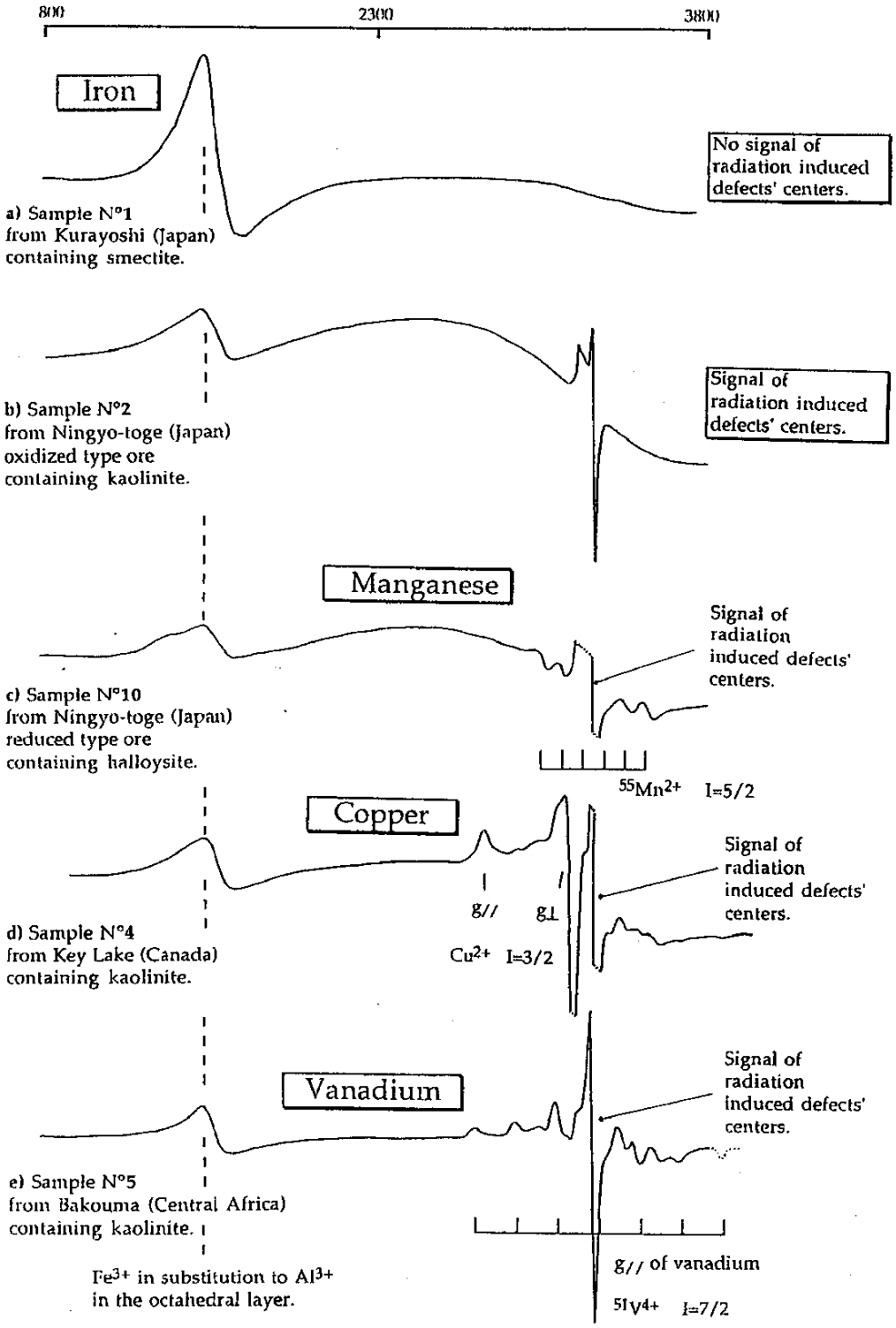


Fig.4 Total ESR spectra of some of the studied samples from U deposits. An example of a ESR spectrum free of radiation defect center signals (a) is given to compare with a typical example of radiation defect center signals around 3300 Gauss (b). $Fe^{3+}$ in substitution to $Al^{3+}$ in octahedral layers can be recognized in many of the samples. Paramagnetic metal species such as Mn (c), Cu (d) and V (e) can be recognized in some of the samples.

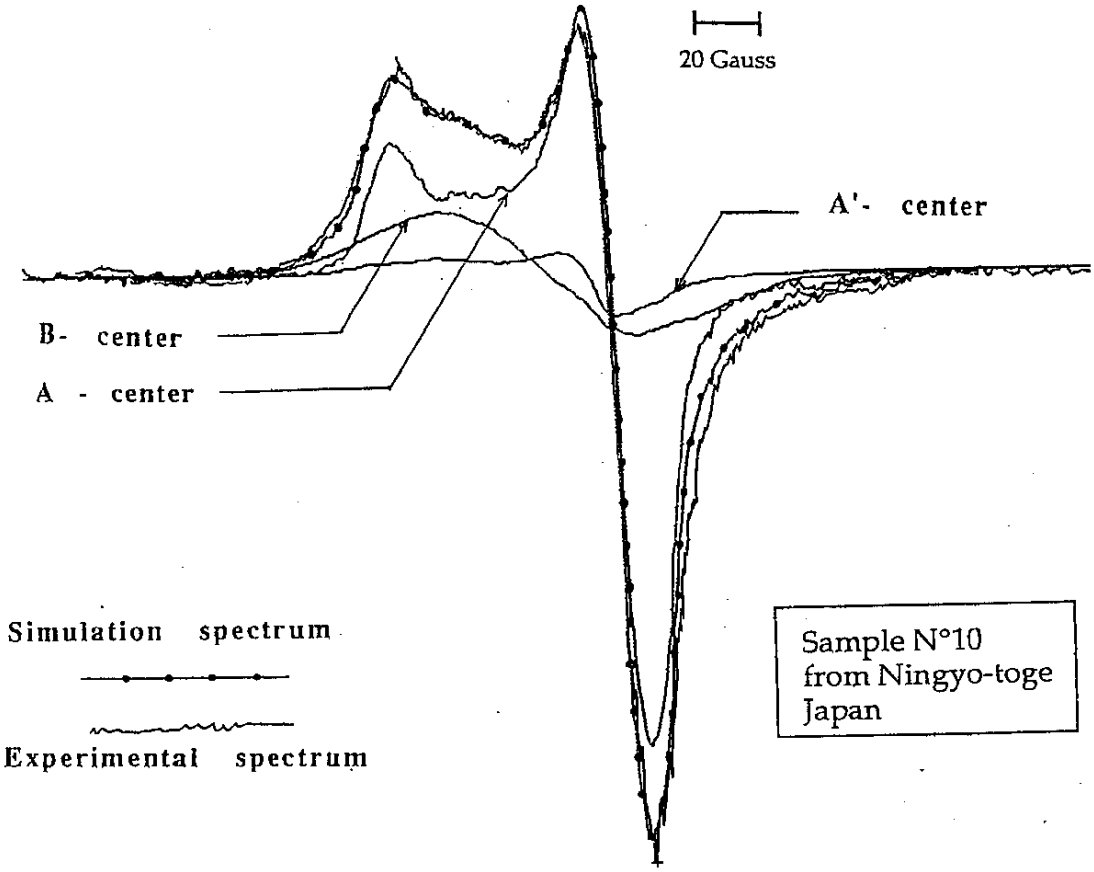


Fig.5 Zoomed and corrected ESR spectra of radiation defect centers for clayish fractions containing halloysite (sample No.10 from Ningyo-toge).The Fe hydroxide and Mn contributions were subtracted from the original spectra (Fig.4c) and the decomposition of total defect signals into A, A′ and B centers is conducted.

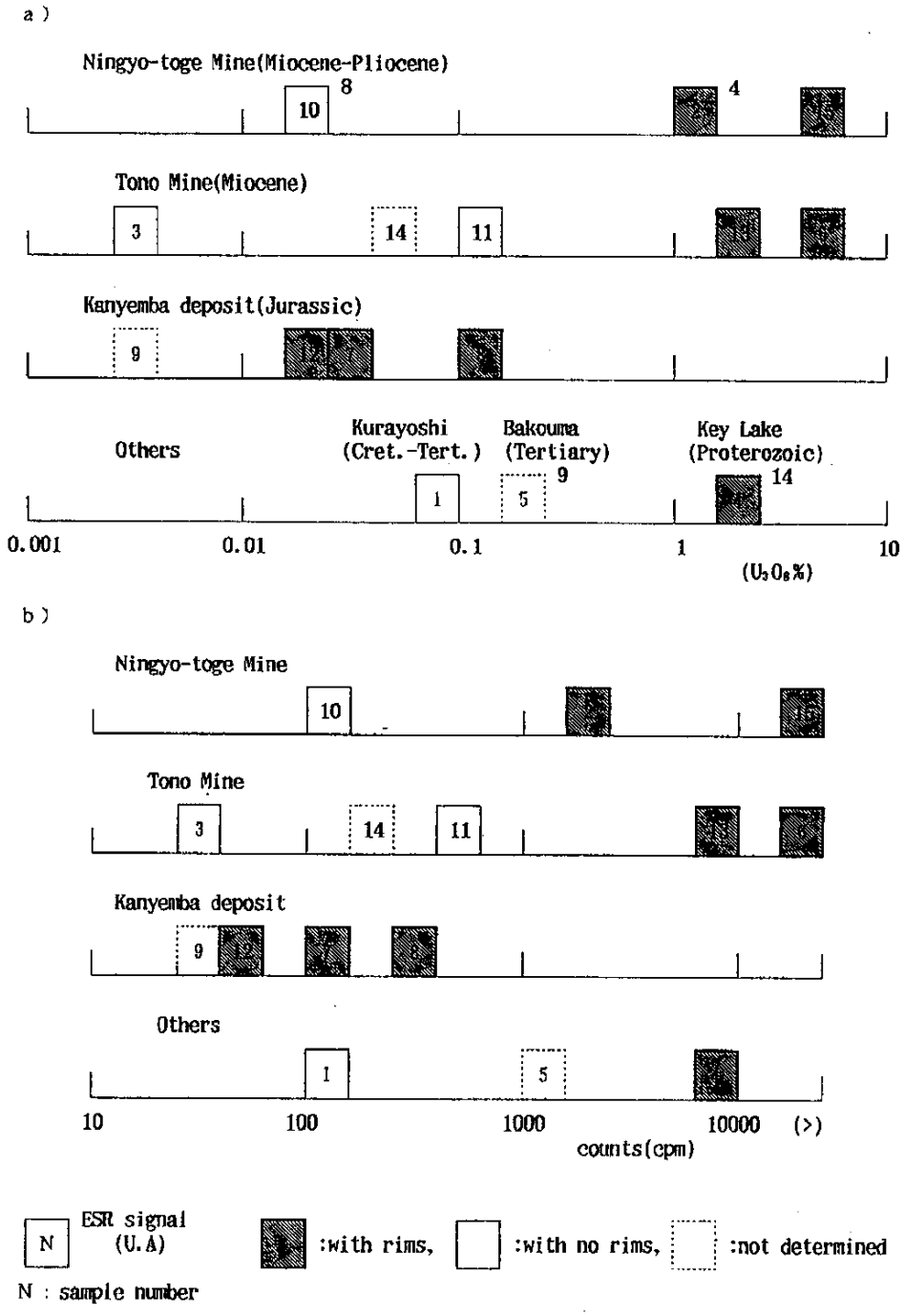


Fig.6 Correlations between the CL rims on quartz grains and the U contents (a) and radioactivities (b) of the studied samples.
Numbers inside the data symbols are the numbers of samples in Tables 1 and 2 and numbers at the right side up corners are the approximate intensities of kaolinite-like radiation centers by ESR (Table 1).

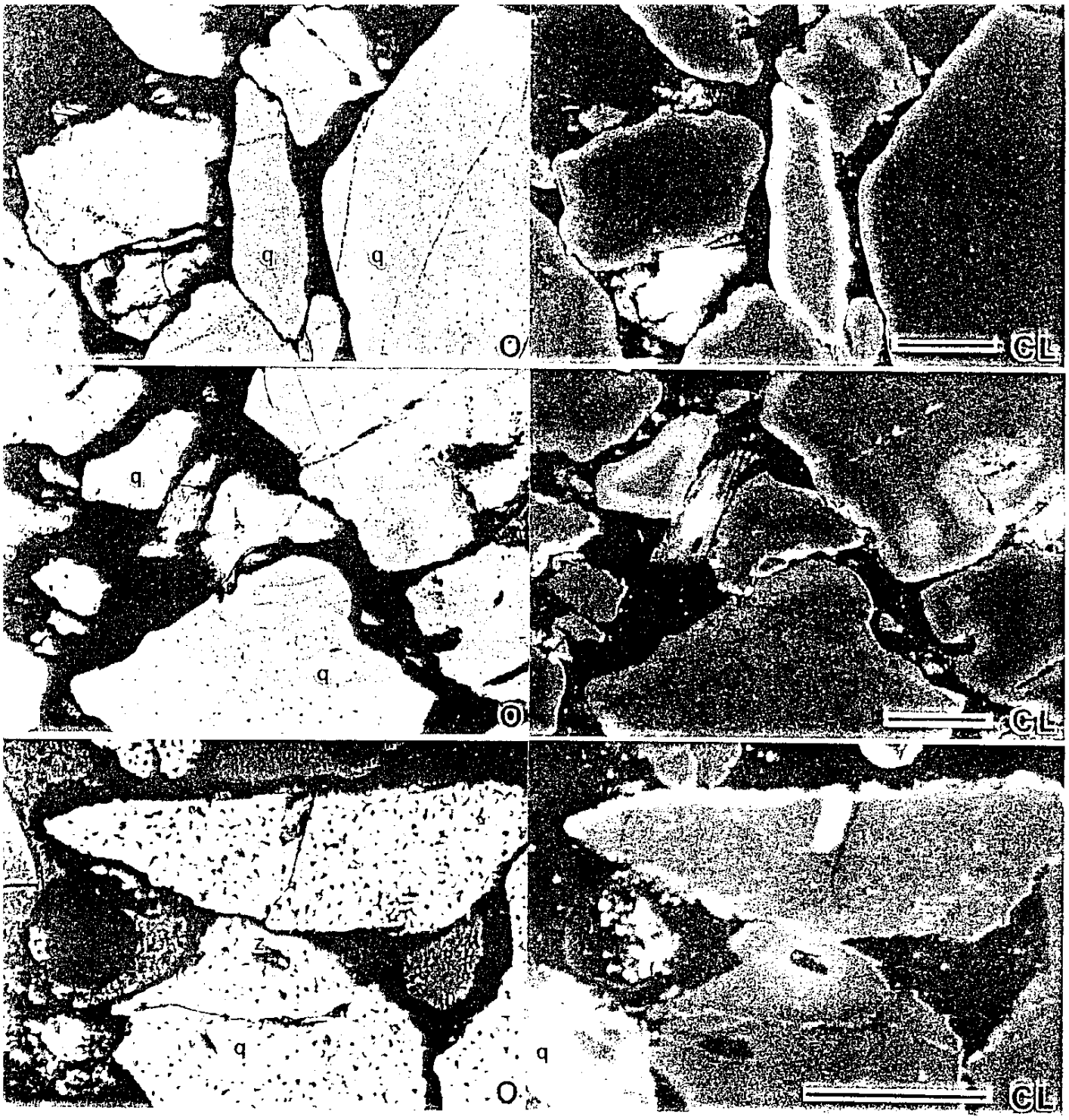


Plate 1 Photomicrographs of polished thin sections from the Kanyemba U deposit. Scale bar is 200 μm.
O: open nicol image under a polarizing microscope;
CL: cathodoluminescence image;
q: quartz, p: plagioclase, kf: alkali feldspar, z: zircon.
(a) Sample No.8. Brownish orange radiation damage rims are generally observed for the surface of reddish brown quartz grains under the CL microscope. Grayish blue rims can also be recognized on some bluish brown quartz grains.
(b) Sample No.8. Zonal structure of radiation damage rims consisting of grayish blue (inside) and brownish orange (outside) parts is noticed on some gray-bluish brown grains.
(c) Sample No.7. Orangish radiation damage rims are observed around zircon in quartz.

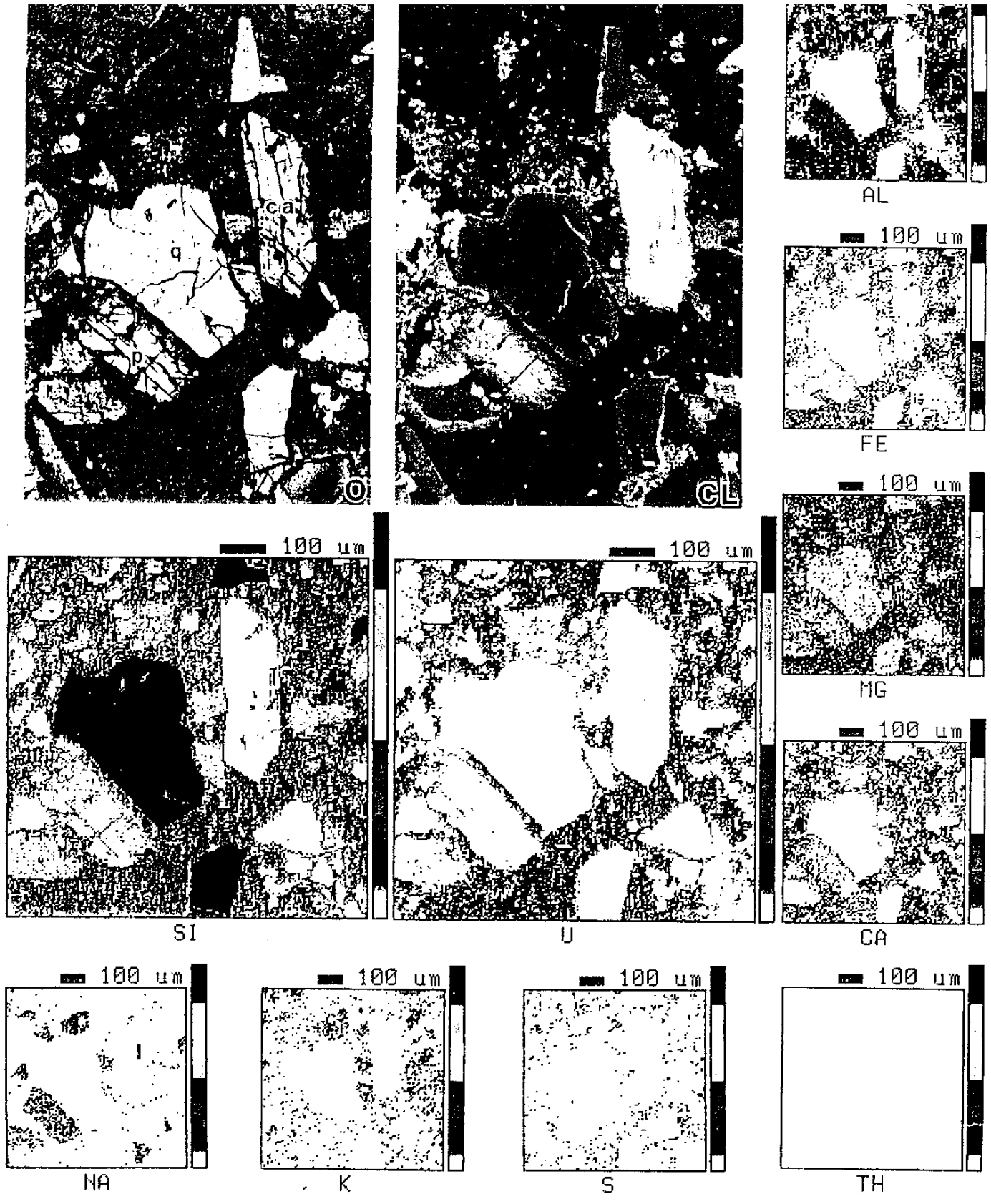


Plate 2 Photomicrographs and compositional mapping of a polished thin section from No.21 outcrop of Tono mine (sample No.6). Scale bars are 100 μm. Pale orangish rims are recognized on reddish brown quartz grains.
O: open nicol image under a polarizing microscope;
CL: cathodoluminescence image;
q: quartz, p: plagioclase, ca: calcite;
Si, U, Na, K, S, Al, Fe, Mg Ca and Th: EPMA mapping images of these elements.

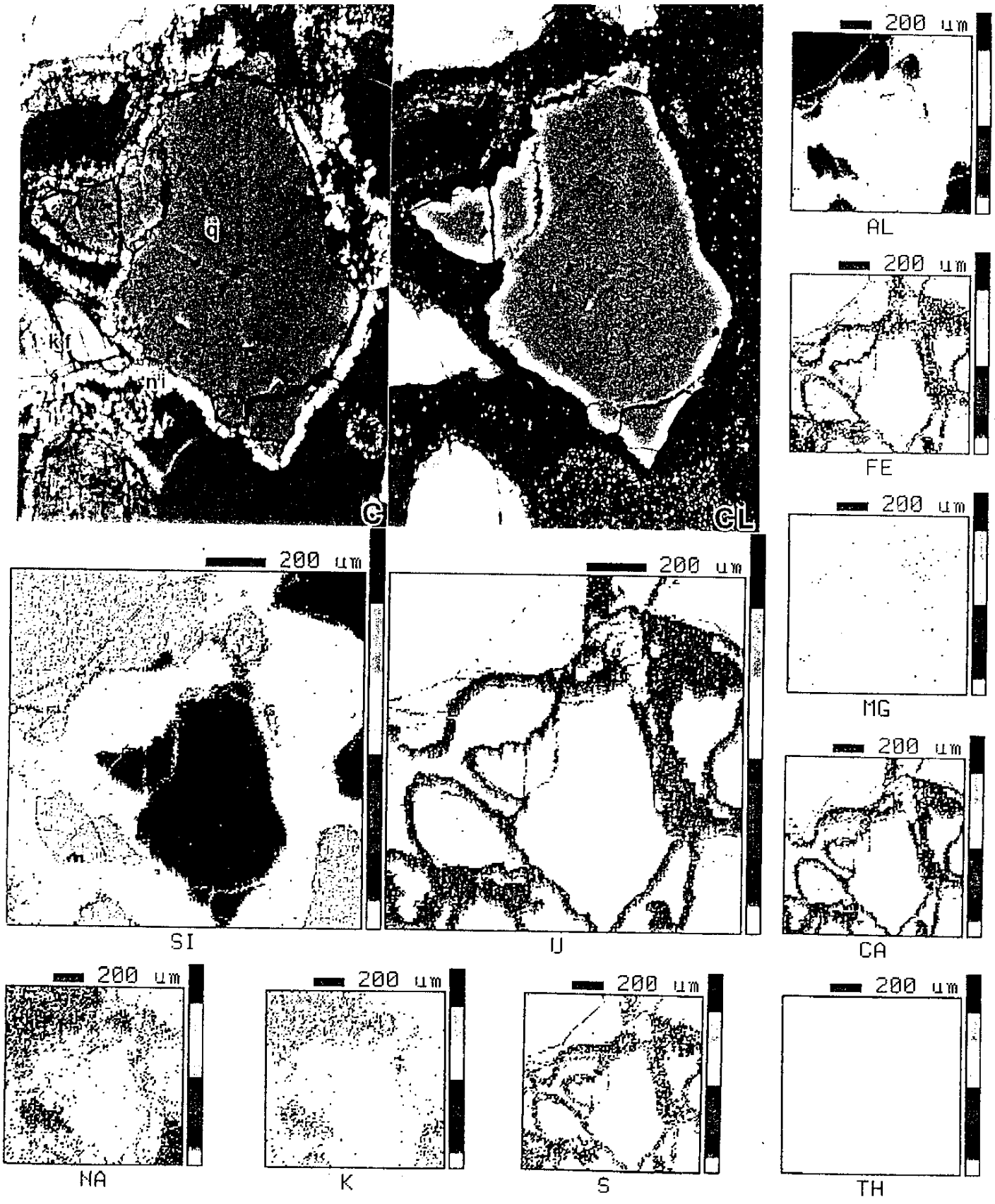


Plate 3 Photomicrographs and compositional mapping of a polished thin section from Nakatsuko deposits, Ningyo-toge mine (sample No.15). Scale bars are 200 μm. Pale orangish rims are recognized on reddish brown quartz grains.
O: open nicol image under a polarizing microscope;
CL: cathodoluminescence image;
q: quartz, kf: alkali feldspar, n: nyngyoite;
Si, U, Na, K, S, Al, Fe, Mg Ca and Th: EPMA mapping images of these elements.

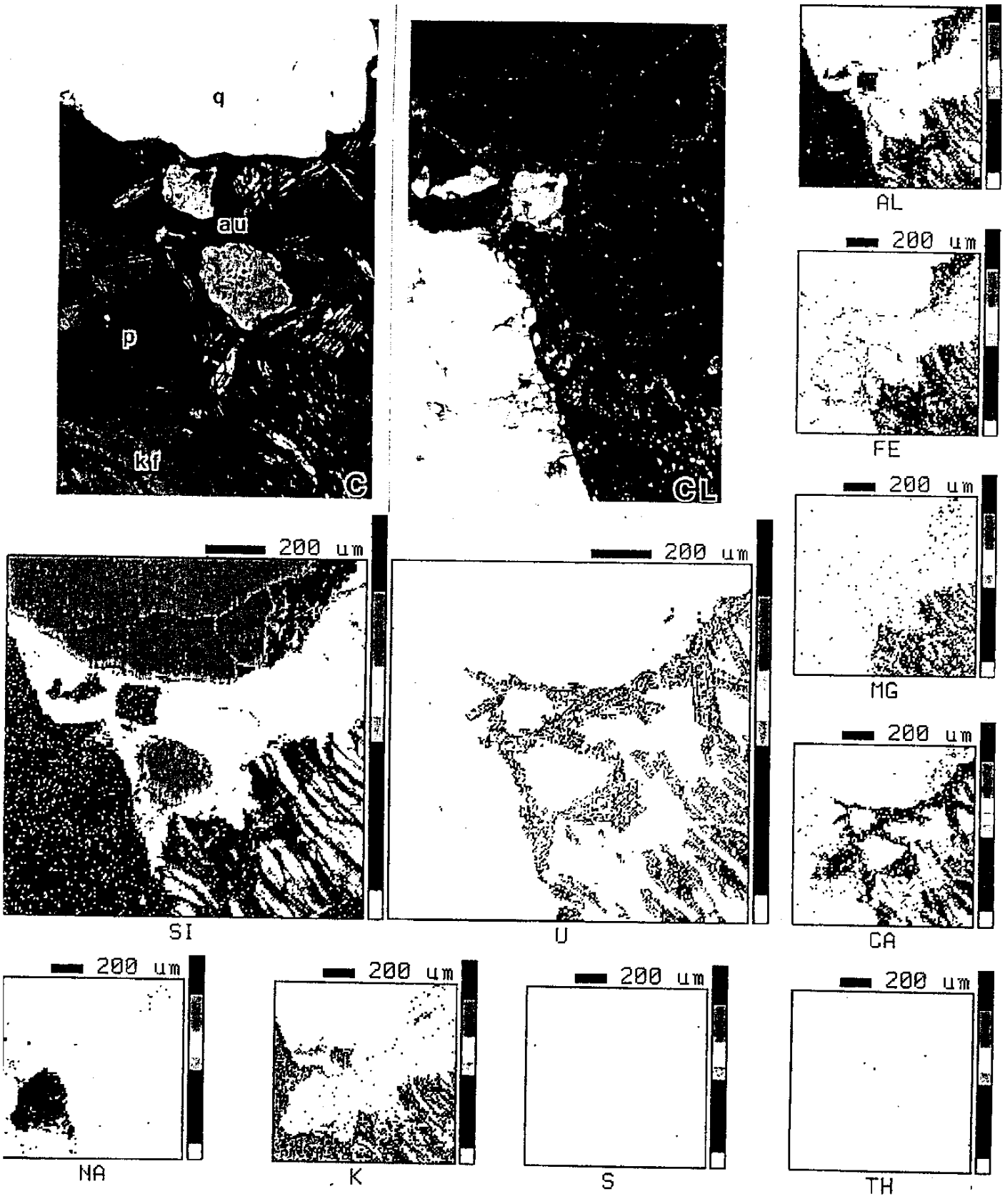


Plate 4 Photomicrographs and compositional mapping of a polished thin section from Yotsugi deposits, Ningyo-toge mine (sample No.2). Scale bars are 200 μm. Pale orangish rims are recognized on reddish brown quartz grains adjacent to metaautunite veins.
O: open nicol image under a polarizing microscope;
CL: cathodoluminescence image;
q: quartz, kf: alkali feldspar, au: metaautunite;
Si, U, Na, K, S, Al, Fe, Mg Ca and Th: EPMA mapping images of these elements.

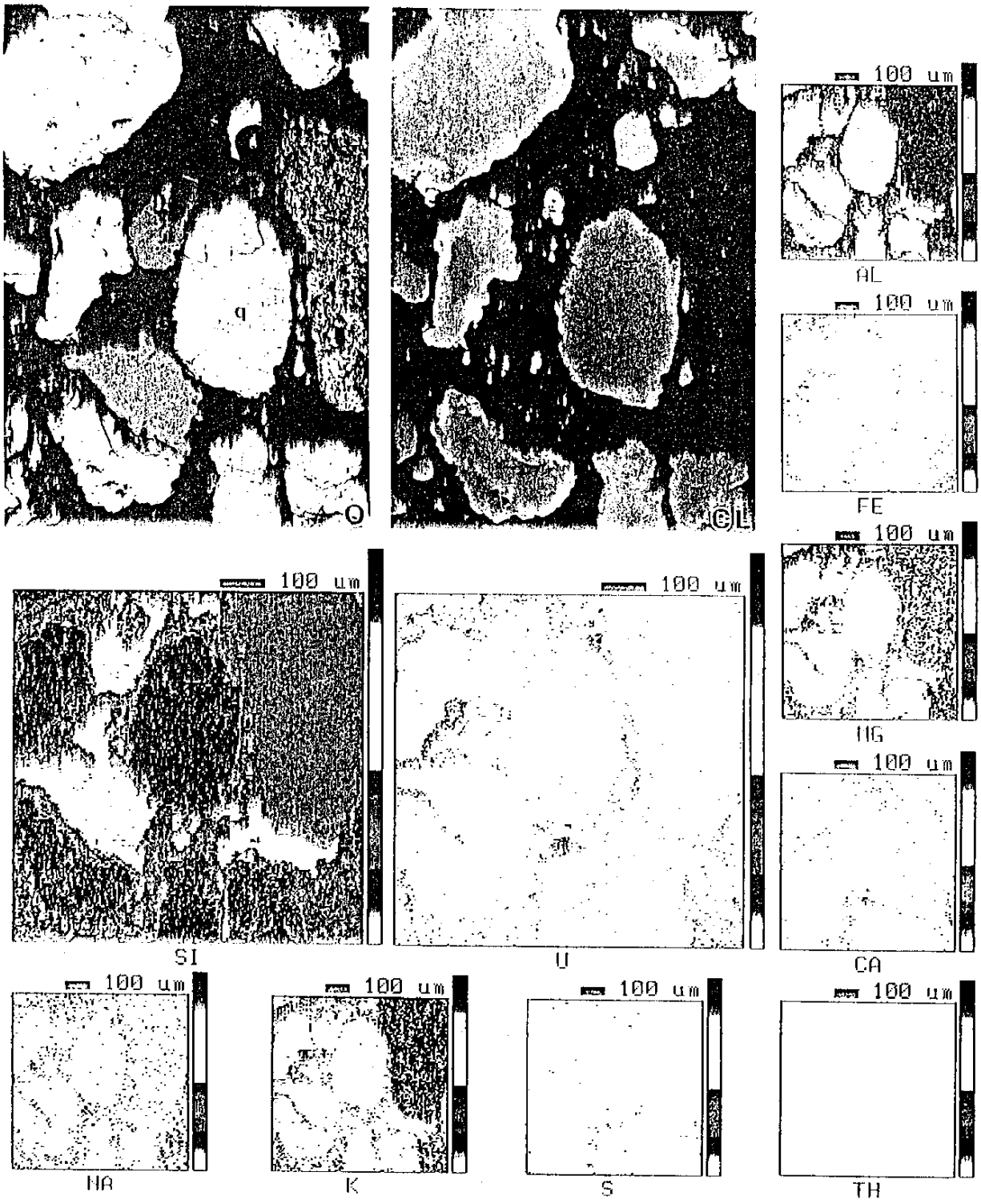


Plate 5 Photomicrographs and compositional mapping of a polished thin section from Key Lake deposits (sample No.4). Scale bars are 100 μm. Brownish orange rims are generally observed for the surface of reddish brown quartz grains under the CL microscope. Grayish blue rims can also be recognized on some bluish brown quartz grains. Zonal structure of radiation damage rims consisting of grayish blue (inside) and brownish orange (outside) parts is noticed on some gray-bluish brown grains.
O: open nicol image under a polarizing microscope;
CL: cathodoluminescence image;
q: quartz;
Si, U, Na, K, S, Al, Fe, Mg Ca and Th: EPMA mapping images of these elements.